Atmos. Chem. Phys. Discuss., 14, 31943–31986, 2014
www.atmos-chem-phys-discuss.net/14/31943/2014/
doi:10.5194/acpd-14-31943-2014

Atmospheric Chemistry and Physics Discussions

Investigation of post-depositional processing of nitrate in East Antarctic snow: isotopic constraints on photolytic loss, re-oxidation, and source inputs

G. Shi[1,2], A. M. Buffen[2], M. G. Hastings[2], C. Li[3], H. Ma[1], Y. Li[1], B. Sun[1], C. An[1], and S. Jiang[1]

[1]Key Laboratory for Polar Science of State Oceanic Administration, Polar Research Institute of China, Shanghai 200062, China
[2]Department of Earth, Environmental and Planetary Sciences and Institute at Brown for Environment and Society, Brown University, Providence, Rhode Island 02912, USA
[3]The State Key Laboratory of the Cryospheric Sciences, Cold and Arid Regions Environmental and Engineering Research Institute, Chinese Academy of Sciences, Lanzhou 730000, China

Received: 25 October 2014 – Accepted: 20 November 2014 – Published: 18 December 2014

Correspondence to: M. G. Hastings (meredith_hastings@brown.edu)

Published by Copernicus Publications on behalf of the European Geosciences Union.

Abstract

Snowpits along a traverse from coastal East Antarctica to the summit of the ice sheet (Dome Argus) are used to investigate the post-depositional processing of nitrate in snow. Seven snowpits from sites with accumulation rates between 24 and 172 $kg\,m^{-2}\,a^{-1}$ were sampled to depths of 150 to 300 cm. At sites from the continental interior (low accumulation, $< 55\,kg\,m^{-2}\,a^{-1}$), nitrate mass fraction is generally $> 200\,ng\,g^{-1}$ in surface snow and decreases quickly with depth to $< 50\,ng\,g^{-1}$. Considerably increasing values of $\delta^{15}N$ of nitrate are also observed (16–461 ‰ vs. air N_2), particularly in the top 25 cm, which is consistent with predicted fractionation constants for the photolysis of nitrate. The $\delta^{18}O$ of nitrate (17–84 ‰ vs. VSMOW), on the other hand, decreases with increasing $\delta^{15}N$, suggestive of secondary formation of nitrate in situ (following photolysis) with a low $\delta^{18}O$ source. Previous studies have suggested that $\delta^{15}N$ and $\delta^{18}O$ of nitrate at deeper snow depths should be predictable based upon an exponential decrease derived near the surface. At deeper depths sampled in this study, however, the relationship between nitrate mass fraction and $\delta^{18}O$ changes, with increasing $\delta^{18}O$ of nitrate observed between 100–200 cm. Predicting the impact of post-depositional loss, and therefore changes in the isotopes with depth, is highly sensitive to the depth interval over which an exponential decrease is assumed. In the snowpits collected closer to the coast (accumulation $> 91\,kg\,m^{-2}\,a^{-1}$), there are no obvious trends detected with depth and instead seasonality in nitrate mass fraction and its isotopic composition is found. In comparison to the interior sites, the coastal pits are lower in $\delta^{15}N$ (−15–71 ‰ vs. air N_2) and higher in $\delta^{18}O$ of nitrate (53–111 ‰ vs. VSMOW). The relationships found amongst mass fraction, $\delta^{15}N$, $\delta^{18}O$ and $\Delta^{17}O$ ($\Delta^{17}O = \delta^{17}O - 0.52 \times \delta^{18}O$) of nitrate cannot be explained by local post-depositional processes, and are instead interpreted in the context of a primary atmospheric signal. Consistent with other Antarctic observational and modeling studies, the isotopic results are suggestive of an important influence of stratospheric chemistry on nitrate formation during the cold season and a mix of tropospheric sources and chemistry during

ACPD
14, 31943–31986, 2014

the warm season. Overall, the findings in this study speak to the sensitivity of nitrate isotopic composition to post-depositional processing and highlight the strength of combined use of the nitrogen and oxygen isotopes for a mechanistic understanding of this processing.

1 Introduction

Nitrate (NO_3^-) is one of the major ions measured in Antarctic snow and ice. In the atmosphere, NO_3^- is formed by oxidation of NO and NO_2, which are collectively referred to as NO_x. In the presence of sunlight, NO and NO_2 recycle rapidly with ozone (O_3), peroxy radical (HO_2) or an organic radical (RO_2), according to the following reactions:

$$NO + O_3 \text{ (or } HO_2 \text{ or } RO_2) \rightarrow NO_2 + O_2 \quad \text{(R1)}$$

$$NO_2 + O_2 \xrightarrow{h\nu} NO + O_3. \quad \text{(R2)}$$

During the day, i.e., when sunlight is present, oxidation of NO_2 by the hydroxyl radical (OH) produces nitric acid (HNO_3):

$$NO_2 + OH + M \rightarrow HNO_3 + M. \quad \text{(R3)}$$

At night and in colder environments, oxidation of NO_2 by O_3 is promoted and HNO_3 can be formed from hydrolysis of dinitrogen pentoxide (N_2O_5),

$$NO_2 + O_3 \rightarrow NO_3 + O_2 \quad \text{(R4)}$$

$$NO_3 + NO_2 + M \leftrightarrow N_2O_{5(g)} + M \quad \text{(R5)}$$

$$N_2O_{5(g)} + H_2O_{(l)} + \text{surface} \rightarrow 2HNO_{3(aq)}, \quad \text{(R6)}$$

or by abstraction of a hydrogen atom by the nitrate radical (NO_3) from dimethyl sulfide (DMS) or a hydrocarbon (HC),

$$NO_3 + \text{DMS or HC} \rightarrow HNO_3 + \text{products}. \quad \text{(R7)}$$

ACPD
14, 31943–31986, 2014

Important NO_x inputs to the troposphere include fossil fuel combustion, biomass burning, soil microbial activity, lightning, and injection from the stratosphere (Delmas et al., 1997; Lee et al., 1997).There has been interest in using ice core NO_3^- records to reconstruct past atmospheric NO_x sources, concentrations and variability over time. Increasing NO_3^- concentrations in Greenland ice core records correspond to increasing fossil fuel and/or agricultural emissions since the Industrial Revolution (Mayewski and Legrand, 1990; Hastings et al., 2009). In contrast, such increases in NO_3^- have not been observed in Antarctica (Wolff, 1995; Wolff et al., 2012), suggesting that concentrations in snow are mainly controlled by natural sources.

The partitioning of NO_x inputs using ice core NO_3^- concentrations is difficult, however, since concentration alone cannot identify specific NO_x sources and NO_3^- can be lost from snow by post-depositional processes such as photolysis and possibly volatilization as HNO_3 (Wolff, 1995; Röthlisberger et al., 2000; Frey et al., 2009). Measurements of nitrogen and oxygen stable isotope ratios in NO_3^- provide further constraints for past NO_x sources and oxidation chemistry (Alexander et al., 2004; Hastings et al., 2009; Hastings, 2010). In the atmosphere, the oxygen isotopes in NO_3^- reflect the isotopic compositions of the oxidants contributing to the production of NO_3^- (e.g., R1-R7 above; Hastings et al., 2003; Michalski et al., 2003; Alexander et al., 2009), and the nitrogen isotopes can reflect NO_x sources and possible imprints of transport and chemistry (Hastings et al., 2003; Elliott et al., 2007; Savarino et al., 2007; Morin et al., 2008; Altieri et al., 2013). However, post-depositional processing in snow can modify the isotopic composition of NO_3^-. At Dome C in East Antarctica (where the snow accumulation rate is roughly $25\,kg\,m^{-2}\,a^{-1}$, i.e., $< 10\,cm\,snow\,a^{-1}$), NO_3^- mass fractions decrease from hundreds of $ng\,g^{-1}$ in surface snow to tens of $ng\,g^{-1}$ at a depth of 10 cm and this decrease corresponds to large changes in isotopic composition (Röthlisberger et al., 2000; Blunier et al., 2005; Frey et al., 2009; Erbland et al., 2013) such that this processing should be identifiable where it occurs. The influence of post-depositional alteration on NO_3^-, however, appears closely related to annual snow accumulation and at

ACPD
14, 31943–31986, 2014

sites with higher accumulation rates, such as Summit, Greenland (200 kg m^{-2} a^{-1}, i.e., 60 cm snow a^{-1}; Dibb and Fahnestock, 2004), the post-depositional effects are rather minor, and the atmospheric signal appears to be preserved (Hastings et al., 2004; Fibiger et al., 2013).

In recent studies, the spatial variability of photolytic and volatile NO_3^- loss in East Antarctic upper snow has been investigated (Frey et al., 2009; Erbland et al., 2013), and represents important progress in understanding air-snow transfer of NO_3^-. However, there are still a number of questions regarding the interpretation of NO_3^- isotopes due to the complicated post-depositional behavior of NO_3^-. Distinguishing the form, extent and relative importance of the different possible isotope effects associated with post-depositional processes is critical for understanding what NO_3^- in an ice core represents.

In this study, samples from 150 to 300 cm-deep snowpits, have been collected at seven sites along a traverse from the East Antarctic coast to Dome Argus (Dome A: the summit of the Antarctic ice sheet), and NO_3^- mass fraction and isotopic composition were determined. The key objectives of this study are: (1) to investigate the effects of post-depositional processes on isotopic composition of NO_3^- at different depths in the snowpack; and (2) to understand the variation of NO_3^- isotopes in different environments across the East Antarctic Ice Sheet (EAIS). The results of this study are of significance to a further understanding of post-depositional processing of snow NO_3^- and the interpretation of NO_3^- isotopic composition archived in ice cores.

2 Materials and methods

2.1 Sample collection

The Chinese National Antarctic Research Expedition (CHINARE) team conducts an annual inland traverse from the coastal Zhongshan Station (Indian Ocean sector) to Dome A in East Antarctica (Fig. 1). This traverse covers a distance of 1250 km. On

ACPD
14, 31943–31986, 2014

the traverse route from Zhongshan to Dome A, seven snowpits were excavated during the 2012/13 austral summer season (Fig. 1). Full information about each pit, including location, snow depth, sampling resolution, collection date, etc., is summarized in Table S1.

Snowpits were excavated manually and one snow wall was scraped clean and flat with a high-density polyethylene (HDPE) scraper. Snow samples were collected using 250 mL narrow-mouth HDPE vials pushed horizontally into the snow wall beginning at the bottom of the pit and moving upwards. The scraper and vials were pre-cleaned with Milli-Q ultrapure water (> 18.2 MΩ), dried in a class 100 super clean hood at 20 °C and then sealed in the clean polyethylene (PE) bags that were not opened until the field sampling started. Field blanks consisting of sampling bottles filled with Milli-Q water were analyzed for ion concentrations. All personnel wore PE gloves and face masks and the pit sites were generally 1 km away from the traverse route to avoid possible contamination from expedition team activities. After collection, the vials were again sealed in clean PE bags and preserved in a clean insulated cabinet. All together, 530 snow samples were collected. All samples were transported to China in a freezer at −25 °C and then shipped frozen to Brown University in Providence, RI.

2.2 Sample analysis

Snow NO_3^- mass fractions (denoted as $w(NO_3^-)$ in the following context) were determined using a Westco Scientific SmartChem 200 discrete chemistry analyzer. The SD (standard deviation) of $w(NO_3^-)$ of 55 field blanks run within sets of samples was 0.8 ng g^{-1}, which is comparable to blank Milli-Q water run on the same system. The pooled SD of samples run in replicate (n = 50) in different sample sets is 1.5 ng g^{-1}.

Snow NO_3^- isotopic compositions were measured according to the denitrifier method by using denitrifying bacteria to convert NO_3^- to N_2O gas, which is collected and injected into a stable isotope ratio mass spectrometer (Thermo Scientific DELTA V Plus; Sigman et al., 2001; Casciotti et al., 2002; Kaiser et al., 2007). At Brown, a minimum

ACPD
14, 31943–31986, 2014

of 5 nmol of NO_3^- is required for an accurate isotopic determination of $^{15}N/^{14}N$ and $^{18}O/^{16}O$ ratios in snow samples with $w(NO_3^-)$ as low as 6.0 ng g^{-1} can be analyzed directly without a pre-concentration step.

NO_3^- isotopic ratios ($\delta^{15}N(NO_3^-)$ and $\delta^{18}O(NO_3^-)$) are defined as

$$\delta = R_{sample}/R_{standard} - 1, \quad (1)$$

where R is $^{15}N/^{14}N$ or $^{18}O/^{16}O$. $\delta^{15}N(NO_3^-)$ and $\delta^{18}O(NO_3^-)$ values are reported in per mil (‰) relative to atmospheric N_2 ($\delta^{15}N_{air} = 0$ ‰) and Vienna Standard Mean Ocean Water (VSMOW $\delta^{18}O = 0$ ‰). All of the isotopic data were calibrated using the international reference materials IAEA-NO-3, USGS-35, USGS-34 and USGS-32 (Michalski et al., 2002; Böhlke et al., 2003). Precision of the isotopic analyses was calculated in two ways. First, the pooled SD ($1\sigma_p$) of all standards run within individual sample sets was calculated, as used in a previous study (Buffen et al., 2014). For $\delta^{15}N(NO_3^-)$, the $1\sigma_p$ of standards is 0.3 ‰ (IAEA-NO-3, $n = 80$), 0.3 ‰ (USGS-34, $n = 80$), 1.1 ‰ (USGS-32, $n = 53$); and for $\delta^{18}O(NO_3^-)$ this is 0.6 ‰ (IAEA-NO-3, $n = 80$), 0.6 ‰ (USGS-34, $n = 80$) and 0.7 ‰ (USGS-35, $n = 80$). Secondly, the pooled SD of all replicate samples run in at least two different sets was examined ($n = 38$) and yielded 0.8 ‰ for $\delta^{15}N(NO_3^-)$ and 0.5 ‰ for $\delta^{18}O(NO_3^-)$. The pooled SD of the replicate samples is probably the most representative measure of precision as it accounts for the total variation within the denitrifier method (i.e., from sample preparation to isotopic determination), and the variance is not diluted compared to the much higher number of standards that are pooled across sample sets (compared to individual samples that are only run once or twice).

During the NO_3^- reduction by bacteria, a small number of oxygen atoms may be exchanged between water and the intermediates of denitrification (e.g., NO_2^-) and must be corrected for the isotopic determination. In general, this exchange is < 10 %, and typically < 3 %, of the total O atoms in the produced N_2O and is corrected for using the measured snow oxygen isotope composition-$\delta^{18}O(H_2O)$ (see Casciotti et al.,

ACPD
14, 31943–31986, 2014

2002; Kaiser et al., 2007 for correction schemes). $\delta^{18}O(H_2O)$ was determined using the standard CO_2 equilibration method (Johnsen et al., 1997). The SD of reference (VSMOW) measurements ($n = 20$) was 0.10 ‰. Full snowpit profiles of $\delta^{18}O(H_2O)$ were only completed for P1 and P7, while only surface snow samples (3 cm) were measured for P2–P6.

A correction is also needed for $\delta^{15}N(NO_3^-)$ to account for the contribution of the $^{14}N^{14}N^{17}O$ isotopologue to the m/z 45 signal measured by the IRMS (Kaiser et al., 2007). Because atmospheric NO_3^- contains a non-zero $\Delta^{17}O$ (i.e., $\Delta^{17}O = \delta^{17}O - 0.52 \times \delta^{18}O > 0$ ‰), simply assuming $\delta^{17}O = 0.52 \times \delta^{18}O$ can yield an overestimate of the true $\delta^{15}N(NO_3^-)$ by as much as 1–2 ‰ (Sigman et al., 2001; Hastings et al., 2003; Savarino et al., 2007). To account for this contribution, a measured or estimated $\Delta^{17}O(NO_3^-)$ is used to correct the $\delta^{15}N(NO_3^-)$ values. Previous East Antarctic investigations have shown that $\Delta^{17}O(NO_3^-)$ mainly ranges from 25 to 35 ‰ in snow NO_3^- (Erbland et al., 2013) and we find a similar range for P1 in our study (see below). For P1, the measured $\Delta^{17}O(NO_3^-)$ values reported below were used to correct $\delta^{15}N(NO_3^-)$, while a mid-range value of $\Delta^{17}O(NO_3^-)$=30 ‰ was used for P2–P7. Using this mid-range value of $\Delta^{17}O(NO_3^-)$=30 ‰ leads to an average $\delta^{15}N(NO_3^-)$ difference of 1.6 ‰ compared to using $\Delta^{17}O(NO_3^-) = 0$ ‰. A difference of ±5 ‰ in the $\Delta^{17}O(NO_3^-)$ used to correct the data (i.e., $\Delta^{17}O(NO_3^-) = 25$ to 35 ‰) results in a $\delta^{15}N(NO_3^-)$ difference of 0.3 ‰, which is comparable to our reported analytical precision and is negligible when compared to the range of sample $\delta^{15}N(NO_3^-)$ values.

For determination of $\Delta^{17}O(NO_3^-)$, the sample N_2O produced by the denitrifier method was thermally decomposed to N_2 and O_2 in a heated gold tube, and the O_2 was then measured at m/z 32 and 33 signals on the IRMS (Kaiser et al., 2007). A minimum of 35 nmol NO_3^- is needed for the analysis, but the low $w(NO_3^-)$ and low sample volumes available in this study limited the measurement of both $\Delta^{17}O(NO_3^-)$ and $\delta^{15}N$ and $\delta^{18}O$ on the same sample. A pre-concentration procedure is needed for the measurement

ACPD
14, 31943–31986, 2014

of $\Delta^{17}O(NO_3^-)$. Briefly, NO_3^- was trapped in an anion exchange resin, and then eluted by a 1 M NaCl solution. A variety of NaCl salts were tested and found to contain NO_3^-, and thus procedural blanks were determined for each batch of NaCl used. (Note that NO_3^- was found in every batch of NaCl (Fisher Scientific) tested, ranged from 478 to 547 ng g^{-1}, and was different even for bottles with the same lot number.) For the samples from P1, 28 ng g^{-1} was measured for the 1 M solution of NaCl used for elution. During the concentrating procedure, one Milli-Q water blank and two sets of standards (USGS-34 and USGS-35) with similar $w(NO_3^-)$ to the snow samples were processed simultaneously. The measured $\Delta^{17}O(NO_3^-)$ was then corrected by two steps: (1) $\Delta^{17}O(NO_3^-)$ in concentrated samples was linearly corrected using the standards USGS-34 and USGS-35 run within individual sample sets; and (2) the output of step (1) was further corrected by the standards used during the concentration procedure to account for the impact of procedural influence (e.g., the NaCl blank). A mean difference of 2.5 ‰ for $\Delta^{17}O(NO_3^-)$ was obtained without the step (2) correction, which means that pre-concentration can result in an underestimation at least on the order of 2.5 ‰ for $\Delta^{17}O(NO_3^-)$.

3 Results

3.1 Snowpit $w(NO_3^-)$

Summary statistics for $w(NO_3^-)$, $\delta^{15}N(NO_3^-)$ and $\delta^{18}O(NO_3^-)$ in each snowpit are given in Table 1 and the detailed profiles are illustrated in Fig. 2. In general, $w(NO_3^-)$ is lower than 200 ng g^{-1} in P1 and P2, which are characterized with higher annual snow accumulation (see Fig. 1), and large, quasi-regular fluctuations of $w(NO_3^-)$ are present in both pits. In contrast, pits P4–P7 from the lower snow accumulation sites show the highest $w(NO_3^-)$ in surface snow, which falls sharply from > 200 ng g^{-1} near the sur-

ACPD
14, 31943–31986, 2014

face to below 50 ng g^{-1} within the top meter, and do not contain regular fluctuations. The markedly decreasing trend of $w(NO_3^-)$ with depth seems to fit an exponential model as has been done previously (Traversi et al., 2009).

3.2 Isotopic compositions of NO_3^-

For $\delta^{15}N(NO_3^-)$ and $\delta^{18}O(NO_3^-)$, the coastal and inland pits differ greatly in terms of the average values and the variability with depth. For the coastal sites P1–P3, $\delta^{15}N(NO_3^-)$ is generally lower than in the inland snowpits P4–P7, varying between −14.8 and 70.8 ‰, while $\delta^{15}N(NO_3^-)$ in the inland pits ranges from 15.5 to 460.8 ‰ (Table 1; Fig. 2). This high value of 460.8 ‰ in pit P7 (which is at Dome A) is the highest natural $\delta^{15}N(NO_3^-)$ on Earth so far reported to our knowledge. In the inland pits (P4–P7), $\delta^{15}N(NO_3^-)$ is lower in the uppermost layers and strongly increases deeper in the snowpack, with most of the increase occurring in the top 25 cm.

In contrast to $\delta^{15}N(NO_3^-)$, $\delta^{18}O(NO_3^-)$ is higher on average in the coastal pits (P1–P3), ranging between 52.5 and 111.2 ‰, compared to the inland sites (P4–P7) where $\delta^{18}O(NO_3^-)$ varies between 16.8 and 84.0 ‰ (Table 1; Fig. 2). It is noted that the averages of $\delta^{18}O(NO_3^-)$ for P4–P7 are comparable, while $\delta^{15}N(NO_3^-)$ means vary significantly, from 133.6 to 335.2 ‰. There is no obvious trend in the $\delta^{18}O(NO_3^-)$ profiles with depth in P1–P3, but this is not the case for the inland sites. $\delta^{18}O(NO_3^-)$ decreases over the top 25 cm, but gradual and consistent increases are observed below 25 cm in P4, P5 and P7 which continue to the pit base (200–300 cm; Fig. 2). A similar decrease in $\delta^{18}O(NO_3^-)$ is observed in the top of P6, but it is not clear if an increasing trend exists in the profile below.

$\Delta^{17}O(NO_3^-)$ of P1 varies from 25.2 to 42.9 ‰, with an average of 32.8 ‰. In general, the variation trend of $\Delta^{17}O(NO_3^-)$ is similar to that of $\delta^{18}O(NO_3^-)$ (Fig. 7), and a close relationship was observed between the two ($r^2 = 0.77$, $p < 0.001$).

ACPD
14, 31943–31986, 2014

4 Discussion

After deposition, NO_3^- can be lost from snow by photolysis or volatilization as HNO_3 (sometimes referred to as evaporation or physical release in other studies), and the extent of loss via these post-depositional processes is accumulation dependent (Röthlisberger et al., 2002; Grannas et al., 2007). At lower accumulation sites, NO_3^- loss is relatively high, synchronous with a large degree of isotopic fractionation (Blunier et al., 2005; Frey et al., 2009; Erbland et al., 2013). In contrast, post-depositional alteration of snow NO_3^- in high accumulation regions can be minor, and seasonal and interannual cycles can be preserved in the snowpack (e.g., Vagenhach et al., 1994; Hastings et al., 2004).

Based on the site differences in annual snow accumulation rate and the profile trends of $w(NO_3^-)$, $\delta^{15}N(NO_3^-)$ and $\delta^{18}O(NO_3^-)$, the seven pits are divided into two groups within the following discussion: group I includes the coastal, medium-high accumulation sites P1–P3 ($> 91\,kg\,m^{-2}\,a^{-1}$) and group II are the low accumulation and further inland sites P4–P7 ($< 55\,kg\,m^{-2}\,a^{-1}$).

4.1 NO_3^- loss in inland upper snowpack: top 25 cm

If it is assumed that post-depositional loss of snow NO_3^- is accompanied by a Rayleigh-type fractionation, the observed changes in $\delta^{15}N$ and $\delta^{18}O$ in a snowpit profile can be described as a function of $w(NO_3^-)$ via

$$\ln(\delta_{snow} + 1) = \varepsilon \cdot \ln(w_{snow}) + [\ln(\delta_{snow,0} + 1) - \varepsilon \cdot \ln(w_{snow,0})], \quad (2)$$

where $\delta_{snow,0}$ and δ_{snow} denote isotopic ratios in the initial and remaining NO_3^-, respectively, and $w_{snow,0}$ and w_{snow} are the initial and remaining NO_3^- mass fractions, respectively (e.g., Blunier et al., 2005). ε can be obtained from the slope of the linear regression for $\ln(w_{snow})$ vs. $\ln(\delta_{snow} + 1)$, while $[\ln(\delta_{snow,0}+1) - \varepsilon \cdot \ln(w_{snow,0})]$ would be the intercept. It is noted that ε is related to the fractionation factor α by $\varepsilon = \alpha - 1$.(Criss, 1999).

ACPD
14, 31943–31986, 2014

Solar radiation decreases exponentially in the snowpack, with attenuation described in terms of an e-folding depth (z_e) where the actinic flux is reduced to $1/e$ (37 %) of the surface value. Accordingly, roughly 95 % of snowpack photochemistry should occur above the depth of three times z_e (Warren et al., 2006). For the individual pits here, we calculate ε values from data in the upper 25 cm, a depth that is close to the z_e calculated by Zatko et al. (2013) for remote Antarctic sites, to evaluate the impacts of post-depositional processes on snow NO_3^- (Table 2). For group II, relatively strong relationships are observed between $w(NO_3^-)$ and $\delta^{15}N(NO_3^-)$ or $\delta^{18}O(NO_3^-)$ in the top 25 cm (as indicated by the r^2 values for Eq. (2) which are higher than 0.44; Table 2). These pits are characterized by negative $^{15}\varepsilon$, with the values of −78.1 ‰ (P4), −84.4 ‰ (P5), −60.6 ‰ (P6) and −59.2 ‰ (P7); whereas $^{18}\varepsilon$ values are positive, indicating a depletion of $^{18}O(NO_3^-)$ with decreasing $w(NO_3^-)$. The observed fractionation constants ($^{15}\varepsilon$ and $^{18}\varepsilon$) for group II (P4–P7) are comparable to those from other snowpits on the East Antarctic plateau (Frey et al., 2009; Erbland et al., 2013).

In the upper 25 cm of the snowpack, a significant NO_3^- loss with increasing depth is seen in the group II pits and corresponds to the large enrichment of $^{15}N(NO_3^-)$. A large loss of NO_3^- leading to such high $\delta^{15}N(NO_3^-)$ values in the surface snow is consistent with the calculated low $^{15}\varepsilon$ in the upper snowpack and our expectations based on other findings in East Antarctica (e.g., Savarino et al., 2007; Erbland et al., 2013). Such strongly positive $\delta^{15}N$ values (> 100 ‰) have not been observed in atmospheric NO_3^-.

4.1.1 Photolytic loss of NO_3^-

Photolysis of snow NO_3^- is thought to primarily occur within a disorder interface, sometimes referred to as a quasi-liquid layer, at the surface of the ice crystal via the reactions

$$NO_3^- + h\nu(+H^+) \rightarrow NO_2 + OH, \quad \text{(R8)}$$

$$NO_3^- + h\nu \rightarrow NO_2^- + O(^3P), \quad \text{(R9)}$$

ACPD
14, 31943–31986, 2014

with Reaction (R8) exceeding Reaction (R9) by a factor of 8–9 (Warneck and Wurzinger, 1988; Dubowski et al., 2001; Chu and Anastasio, 2003). Snow NO_3^- photolysis products are mainly NO_2, greatly exceeding NO under most conditions (Dibb et al., 2002). Under acidic conditions (pH < 5), $HONO_{(g)}$ can also be released (Grannas et al., 2007 and references therein). Only NO_2 produced near the ice surface–air interface can be released to the firn air and subsequently escape from the snowpack to the overlying atmosphere (Boxe et al., 2005).

In order to identify the relative importance of photolysis and volatilization (Sect. 4.1.2) on NO_3^- loss, the fractionation constant of each process should first be quantified. Frey et al. (2009) proposed a theoretical model that has provided a useful approximation of photolytic fractionation. The photolysis rate constant $j_{NO_3^-}$ (s^{-1}) can be expressed as

$$\varphi j_{NO_3^-} = \int \sigma_{NO_3^-}(\lambda, T) \times \phi_{NO_3^-}(\lambda, T, \mathrm{pH}) \times I(\lambda)\mathrm{d}(\lambda), \quad (3)$$

where $\sigma_{NO_3^-}$ (cm^2) is the spectral absorptivity (Chu and Anastasio, 2003); $\varphi_{NO_3^-}$ is the quantum yield (0–1), which was calculated to be 1.7×10^{-3} at 239 K and pH = 5 (Chu and Anastasio, 2003), and I is the spectral actinic flux (photons $cm^{-2}\,s^{-1}\,nm^{-1}$), here taken from the Tropospheric Ultraviolet and Visible (TUV) radiation transfer model (Madronich and Flocke, 1998). The isotopic fractionation constant can then be calculated by

$$\varepsilon = (j/j') - 1, \quad (4)$$

where j corresponds to the heavy isotopologue (e.g., $^{15}N^{16}O_3$), and j' corresponds to the light isotopologue (e.g., $^{14}N^{16}O_3$).

Under peak summer radiation conditions (solstice solar noon), $^{15}\varepsilon$ and $^{18}\varepsilon$ of photolysis are calculated to be between −45.3 ‰ (P1) and −48.0 ‰ (P7) and from −32.5 ‰ (P1) to −34.4 ‰ (P7), respectively. The negative ε values suggest that photolysis will lead to a strong enrichment of both ^{15}N and ^{18}O in NO_3^- remaining in the snow. For $^{15}\varepsilon$

ACPD
14, 31943–31986, 2014

calculated from observations in the upper 25 cm of the group II pits (Table 2), the higher r^2 values imply that photolysis can largely explain enrichment of ^{15}N with the decrease of $w(NO_3^-)$. At Dome C, where snow accumulation is typically less than 50 kg m^{-2} a^{-1}, close to the values of P4–P7 (Fig. 1), photolysis has also been reported as responsible for changes in $\delta^{15}N(NO_3^-)$ in the upper snowpack (Frey et al., 2009; Erbland et al., 2013).

4.1.2 Re-oxidation effects

If the post-depositional loss of NO_3^- in the group II pits was driven solely by photolysis, ^{18}O should also be enriched in the remaining NO_3^- according to the modeled photolytic $^{18}\varepsilon$ values (−32.5 to −34.4 ‰). However, $\delta^{18}O$ decreases over the top 25 cm (Fig. 2) and $^{18}\varepsilon$ values calculated from the observed data in the upper 25 cm are instead positive, varying from 15.6 to 28.8 ‰ (Table 2). Furthermore, simple photolysis will lead to a linear relationship of $\delta^{18}O(NO_3^-)$ vs. $\delta^{15}N(NO_3^-)$ with a slope of roughly 0.7, i.e., equal to the ratio of the fractionation constants. However, there are negative relationships between $\delta^{18}O(NO_3^-)$ and $\delta^{15}N(NO_3^-)$ in the top 25 cm (Fig. 3), with slopes varying from −0.4 to −0.2.

Similar negative relationships have been observed in other East Antarctic snowpits (Frey et al., 2009; Erbland et al., 2013) and, following from experimental and theoretical work (McCabe et al., 2005; Jacobi and Hilker, 2007), were attributed to the aqueous-phase re-oxidation of the products of NO_3^- photolysis (e.g., NO_2) by OH and/or H_2O to form "secondary" NO_3^-.

In this way, the O atoms from OH/H_2O provide a depleted ^{18}O source while $\delta^{15}N(NO_3^-)$ is not affected. For the group II pits, $\delta^{18}O(H_2O)$ in surface snow falls roughly in the range of −45 to −60 ‰. These effects should be considered in explaining the observed positive $^{18}\varepsilon$ values and negative relationships between $\delta^{18}O(NO_3^-)$ and $\delta^{15}N(NO_3^-)$ in the top 25 cm. (Direct exchange of O atoms between NO_3^- and H_2O is

ACPD
14, 31943–31986, 2014

only thought to be important at NO_3^- concentrations that are orders of magnitude higher than those found in snow (Bunton et al., 1952)).

For the top 2.5 cm of snow in P7, $w(NO_3^-)$ and $\delta^{18}O(NO_3^-)$ is 374 ng g^{-1} and 74.9 ‰ respectively, while $w(NO_3^-)$ decreases to 40 ng g^{-1} at a depth of 25 cm. Based on the modeled effect of photolysis, $\delta^{18}O$ in the remaining NO_3^- at 25 cm could be predicted by

$$\delta^{18}O_{remaining} = (1 + \delta^{18}O_0) \cdot f^{(^{18}\varepsilon)} - 1, \quad (5)$$

where $\delta^{18}O_{remaining}$ represents $\delta^{18}O$ in the remaining NO_3^-; $\delta^{18}O_0$ is that of initial NO_3^-; f is the fraction of NO_3^- remaining in the snow; and $^{18}\varepsilon$ is the photolysis fractionation constant (−34.4 ‰). If photolysis alone is responsible for the NO_3^- loss, $\delta^{18}O(NO_3^-)$ is expected to be 161 ‰ at 25 cm and thus the observed $\delta^{18}O$ of 38.4 ‰ requires a cumulative 55 % exchange of O atoms in the remaining NO_3^- assuming a $\delta^{18}O(H_2O)$ of −60 ‰. This is a substantial exchange of O atoms, indicating that re-oxidation plays a major role in determining the $\delta^{18}O$ of NO_3^- in the upper snowpack.

4.1.3 Volatilization

Volatilization, or physical release, of HNO_3 may also be a pathway for post-depositional loss of NO_3^- in snow (Röthlisberger et al., 2000; Erbland et al., 2013). The importance of this process is unclear, however, as loss proceeds only as HNO_3,

$$H^+_{(aq)} + NO^-_{3\,(aq)} \leftrightarrow HNO_{3(aq)} \leftrightarrow HNO_{3(g)}, \quad (R10)$$

and thus requires highly acidic conditions given the very high dissociation constant for HNO_3 (Sato et al., 2008). Volatilization may also be inhibited at low temperatures as suggested by laboratory and field observations (Erbland et al., 2013; Berhanu et al., 2014).

ACPD
14, 31943–31986, 2014

The current understanding of the isotopic impact of volatilization is also uncertain. An experiment conducted by Erbland et al. (2013) at Dome C suggested that the $^{15}\varepsilon$ (mean $\pm 1\sigma$) for volatilization varied from 0.9 ± 3.5 ‰ (−30 °C) to -3.6 ± 1.1 ‰ (−10 °C) (i.e., close to non-fractionating). No observational or experimental data for $^{18}\varepsilon$ are available. Theoretical model estimates of volatile fractionation, assuming that the aqueous-phase equilibrium in R10 is the controlling step in the overall fractionation (Frey et al., 2009), predict values of $^{15}\varepsilon$ and $^{18}\varepsilon$ to be from 12.6 ‰ (0 °C) to 16.8 ‰ (−73 °C) and between 1.1 ‰ (0 °C) and 0.6 ‰ (−73 °C), respectively (Table S2).

For the summertime temperatures at the P4–P7 sites (< −30 °C), physical release should deplete both ^{15}N and ^{18}O in the remaining snow NO_3^- according to the modeled ε values, whereas the field experiment observations would suggest negligible change in δ^{15}N with decreasing $w(NO_3^-)$ in the snow. The observations for P4–P7 show increasing $\delta^{15}N(NO_3^-)$ with decreasing $w(NO_3^-)$, and that $\delta^{15}N(NO_3^-)$ is negatively correlated with $\delta^{18}O(NO_3^-)$ (Fig. 3), disagreeing with both expectations (i.e., field experiment observations and modeled results; Table S2). The current understanding of volatile fractionation, however, is very limited and experimental data for $^{18}\varepsilon$ are not available to date. Nevertheless, little evidence is found to support a significant influence of volatilization at our sites given the existing state of knowledge.

4.2 Isotopic fractionation in deeper snow at inland sites

Fractionation constants and the isotopic relationships with $w(NO_3^-)$ were also examined in two deeper layers (25–100 and 100 cm–pit base) to assess possible variability with depth. As shown in Table 2, the logarithmic relationships between δ^{15}N or δ^{18}O and mass fraction of NO_3^- are strongest in the upper 25 cm, as seen in the r^2 values, but are weaker in the layers below. Interestingly, this loss of a relationship is more noticeable in $\delta^{18}O(NO_3^-)$ than $\delta^{15}N(NO_3^-)$. Interestingly, while $\delta^{15}N(NO_3^-)$ maintains a negative relationship with $w(NO_3^-)$ at all depths, the relationships between $\delta^{18}O(NO_3^-)$ and $w(NO_3^-)$ shift from being positive in the upper 25 cm to generally negative in the deeper

ACPD
14, 31943–31986, 2014

snow (Fig. 4). This leads to there generally being no association between $w(NO_3^-)$ and $\delta^{18}O(NO_3^-)$ when the entire snowpit depth interval is considered (Table 2).

It is also useful to discuss this variability with depth in terms of the isotopic fractionation constants. If it is expected that only one isotopically fractionating process in the snow, such as photolysis, was responsible for post-depositional changes in $\delta^{15}N(NO_3^-)$ and $\delta^{18}O(NO_3^-)$, their respective fractionation constants should be similar at all depths. This is to say that the isotopic imprint of photolysis should be set in the upper snowpack and then preserved below. Also, $\delta^{15}N(NO_3^-)$ and $\delta^{18}O(NO_3^-)$ should not change once NO_3^- is moved below the photic zone. (Stemming from these expectations, the isotopic composition of buried NO_3^- could be back-calculated to that originally at the surface if the isotopic imprint of alteration at the surface could be quantified in terms of a fractionation constant.)

In contrast to this expectation, the calculated ε value is largely dependent on the depth range chosen. Figure 4 illustrates changes in the observed fractionation constants with depth in the group II snowpits. Both $^{15}\varepsilon$ and $^{18}\varepsilon$ vary but with distinct differences. The $^{15}\varepsilon$ tends to become more positive with depth, while $^{18}\varepsilon$ decreases and even switches from positive to negative values. When taken together with variability in the strength of the relationships with $w(NO_3^-)$ (Table 2) and the observation that isotopic composition continues to change below the expected photic zone depths, especially for $\delta^{18}O(NO_3^-)$ (Fig. 2), it seems that a single process does not adequately explain post-depositional alteration at these inland sites. Instead, it appears that the effects on $w(NO_3^-)$, $\delta^{15}N(NO_3^-)$ and $\delta^{18}O(NO_3^-)$ vary with depth.

How could this occur? The lifetime of NO_x in snow should be determined by escape to the overlying atmosphere (wind pumping, convection and diffusion) and also by chemical conversion back to NO_3^- in the firn air, which may then be re-deposited (Zatko et al., 2013). Based on the discussion in Sect. 4.1, the positive $^{18}\varepsilon$ values for the upper 25 cm of snow can be explained by secondary NO_3^- formation in the condensed phase (some products are lost to the gas phase while those remaining are involved

ACPD
14, 31943–31986, 2014

in re-oxidation reactions where O atoms from OH and/or H_2O are incorporated into this secondary NO_3^-). This can explain the positive relationship between $\delta^{18}O(NO_3^-)$ and $w(NO_3^-)$ in the upper snow (Fig. 5). Deeper in the snow, however, it is possible that this relationship is lost because NO_x does not escape the snowpack but is instead converted back to NO_3^- in the interstitial firn air and then re-deposited. In this case, the increase in $\delta^{18}O(NO_3^-)$ with depth in the group II pits could potentially be explained by oxidation of NO_x by O_3 in the firn air. O_3 imparts a high positive $\delta^{18}O$ signature (on the order of 130 ‰, Vicars and Savarino, 2014), while other possible sources of O such as H_2O, OH or O_2 are considerably lower in $\delta^{18}O$ (e.g., > −60 ‰ to 24 ‰).

Such changes with depth have not previously been observed in inland East Antarctica. In the work of Erbland et al. (2013), 10 of 11 snowpits from the plateau were not sampled below 50 cm depth, while the group II pits in this work were continuously sampled down to 200–300 cm. It is possible that sampling did not extend deep enough in the Erbland et al. (2013) study to capture this change in $\delta^{18}O(NO_3^-)$. However, the expectation would be that 50 cm should well cover the extinction of light into the snowpack (e.g., 50 cm is a greater than 3 times the *e*-folding depth at Dome C), and therefore below this depth the isotopes should no longer be influenced by photolytic conversion of NO_3^- to NO_x. Another possible explanation could be that the ventilation depths (where NO_x is predominantly lost from the firn to the overlying atmosphere) are shallower and/or that light penetration is deeper at Dome A and the group II sites compared to previously sampled inland East Antarctic sites. Ventilated depths are dependent on a variety of firn properties that affect densification, porosity and air exchange (e.g., Zatko et al., 2013). If gas-phase re-oxidation of NO_x in the deeper snowpack of only some inland Antarctic sites is substantial, this would add additional complexity to the interpretation of ice core NO_3^- records from sites with extensive photolytic influence.

So far, the direct observations of nitrogen compounds and oxidants in interstitial air are very limited. Concentrations of NO_x, HONO, HNO_3, H_2O_2, etc., have been measured in the upper snowpack (e.g., the top 10 cm) in Antarctica (Hutterli et al., 2004; Frey et al., 2013; Legrand et al., 2014), however, interstitial air in the deeper snowpack

ACPD
14, 31943–31986, 2014

(e.g., > 100 cm in depth) has never been measured for mixing ratios of O_3, OH, NO_x and HNO_3. Such measurements in deeper snow would be helpful in answering whether or not NO_x/NO_3^- undergoes other reactions at these deeper depths.

4.3 Predicting $w(NO_3^-)$, $\delta^{15}N(NO_3^-)$ and $\delta^{18}O(NO_3^-)$ values in buried snow

Erbland et al. (2013) proposed that snow $w(NO_3^-)$ and isotopic compositions may approach constant values, called "asymptotic" values, below the photic zone (or zone of active NO_3^- loss). By means of an exponential decrease regression, asymptotic values are calculated by

$$M(x) = M_{(as.)} + [M_{(0)} - M_{(as.)}] \times \exp(-c \times x), \quad (6)$$

where $M_{(x)}$ is the $w(NO_3^-)$, $\delta^{15}N(NO_3^-)$ or $\delta^{18}O(NO_3^-)$ at depth x (cm); $M_{(as.)}$ is the asymptotic value for these parameters; $M_{(0)}$ is the value at the surface of the snowpit; and c is a constant. Asymptotic values for each snowpit are calculated from the best fit (minimizing the sum of squared residuals) of $M_{(x)}$ vs. depth.

As seen in Fig. 2 and discussed above, $w(NO_3^-)$, $\delta^{15}N(NO_3^-)$ and $\delta^{18}O(NO_3^-)$ do not achieve constant values in the deeper snow layers of group I pits. As a result, it would be unreasonable to calculate asymptotic values for these pits based on an exponential decrease regression. On the contrary, variance in $w(NO_3^-)$, $\delta^{15}N(NO_3^-)$ and $\delta^{18}O(NO_3^-)$ in the deeper snowpack of the group II pits is relatively small. In order to compare the asymptotic values derived from different snow depth ranges, observations from five intervals (0–25 cm, 0–60 cm, 0–80 cm, 0–100 cm, and the entire pit) were selected to make this calculation and the results are listed in Table 3. An illustration of the sensitivity of the calculation of asymptotic values for different depth intervals in a single snowpit is shown in the Supplement (Fig. S1).

For a clear comparison across the snowpits, the five asymptotic values for each snowpit are displayed in Fig. 6. The averages of observed data in the bottom 20 cm of each pit (denoted as $w(NO_3^-)_{(av.)}$, $\delta^{15}N_{(av.)}$ and $\delta^{18}O_{(av.)}$ in the following context) are

ACPD
14, 31943–31986, 2014

also shown in Fig. 6 to check the agreement with the predicted asymptotic values. With regards to $w(NO_3^-)_{(as.)}$, the values calculated using the 0–25 cm layer are typically higher than those using the deeper depth intervals, which is expected since $w(NO_3^-)$ continues to decrease below 25 cm (Fig. 2). The values of $w(NO_3^-)_{(as.)}$ calculated from the 0–100 cm interval and those using the entire snowpit are close to $w(NO_3^-)_{(av.)}$ on the whole, indicating a better prediction. The values of $\delta^{15}N_{(as.)}$ obtained from the 0–25 cm interval are generally lower than those calculated using the entire pit and 0–100 cm. $\delta^{15}N_{(av.)}$ is roughly close to the $\delta^{15}N_{(as.)}$ values calculated from 0–100 cm and from the entire pit, similar to the pattern for $w(NO_3^-)$. In contrast, $\delta^{18}O_{(av.)}$ is generally higher than the values of $\delta^{18}O_{(as.)}$, implying that $\delta^{18}O(NO_3^-)$ in deeper snow is more difficult to predict compared to $w(NO_3^-)$ and $\delta^{15}N(NO_3^-)$. This conclusion is consistent with the changes in $\delta^{18}O$ at deeper depths as discussed in Sect. 4.2.

In cases where there is significant post-depositional loss and/or processing of NO_3^-, the $\delta_{(as.)}$, in theory, could help account for the impact of post-depositional processing compared to preservation in reconstructing a primary atmospheric signal. Our results clearly show that $\delta_{(as.)}$ is sensitive to the depth interval over which exponential decrease is assumed. As seen in Fig. 2 and discussed in the next section, pit profiles from the high accumulation sites in group I do not fit an exponential decrease function, but instead show periodic variability in mass fraction and isotopic composition of NO_3^-.

4.4 Seasonal shifts in NO_3^- sources to coastal snow

As discussed above, sharp decreases in $w(NO_3^-)$ in the top few centimeters of inland East Antarctic snowpits are interpreted as evidence of severe photolytic NO_3^- loss. $w(NO_3^-)$ in the top 10 cm of the coastal P1 snowpit also decreases from the surface (Fig. 2) and, if viewed in isolation, could also be taken as evidence for post-depositional loss. However, annual average snow accumulation at P1 is approximately 50 cm snow a^{-1}, and the full profile clearly shows that similarly high $w(NO_3^-)$ values are observed

ACPD
14, 31943–31986, 2014

below 10 cm, as would be expected from seasonal cycles. We expect that if the coastal sites studied by Erbland et al. (2013) had been continuously sampled below 20 cm, similar features would have been observed. This should serve as caution in interpreting the behavior of NO_3^- at high accumulation sites based on observations that do not cover a full annual cycle of snowfall.

Profiles of the group I pits (P1–P3) show large variations in $w(NO_3^-)$ and isotopic composition throughout the snowpack, with some correspondence to $\delta^{18}O(H_2O)$ which is a proxy for temperature (Fig. 7). The seasonality is most apparent at site P1 due to the highest sampling resolution (3.0 cm per sample compared to 5.0 cm per sample for pits P2 and P3) and highest snow accumulation rate (172 kg m^{-2} a^{-1}), though all group I sites feature high accumulation rates above 91 kg m^{-2} a^{-1} (Table S1).

It is difficult to assign samples to four distinct seasons based on $\delta^{18}O(H_2O)$ alone, so we choose a conservative classification of two periods: a warm season corresponding to higher $\delta^{18}O(H_2O)$ and a cold season characterized by lower $\delta^{18}O(H_2O)$ (Fig. 7). These assignments are also consistent with other established seasonal tracers measured in P1 in that the $\delta^{18}O(H_2O)$ peaks (warm season) correspond to spikes in MSA and low Na^+, while the opposite pattern is present during the identified cold seasons (C-J. Li, personal communication, 2014). The snow accumulation rate of 172 kg m^{-2} a^{-1} at P1 site, which corresponds to 43–57 cm snow a^{-1} assuming a typical snow density of 0.3–0.4 g cm^{-3}, also fits with the thickness of the designated seasonal layers. Although coarse, this conservative dating of the snowpit is sufficient to make broad comparisons throughout the year. This is aided by the high accumulation rate and the large amplitude variability in the data.

The samples and data assigned to warm and cold seasons for P1 are shown in Figs. 7 and 8. If the $\delta^{18}O(H_2O)$ peaks are taken to roughly correspond with the middle of the warm season, this results in 61 % of samples falling into the cold season compared with the warm season, which agrees well with the seasonal precipitation climatology where conditions slightly favor cold season accumulation (e.g., about 60 % of snow occurs in cold season on coast, Laepple et al., 2011).

ACPD
14, 31943–31986, 2014

As illustrated in Fig. 7, snow $w(NO_3^-)$ spikes are present during the warm periods, while $w(NO_3^-)$ in the cold season is lower. The averages of $w(NO_3^-)$ in warm and cold seasons are 62.0 and 36.6 ng g^{-1}, respectively (Fig. 8). These seasonal cycles in mass fraction are consistent with previous observations at other coastal sites (Mulvaney et al., 1998; Wagenbach et al., 1998; Wolff et al., 2008). In contrast, values of $\delta^{15}N$, $\delta^{18}O$ and $\Delta^{17}O$ of NO_3^-, are all higher in cold seasons (with means of 31.0, 86.3 and 34.4 ‰, respectively); while the averages in warm seasons are 15.1, 77.4 and 30.4 ‰, respectively.

Photolytic loss of NO_3^- at high accumulation sites such as Summit, Greenland (where the 200 kg m^{-2} a^{-1} accumulation rate is comparable to P1) appears to be negligible (Hastings et al., 2004; Fibiger et al., 2013). In addition, the expected negative relationship between $w(NO_3^-)$ and $\delta^{15}N(NO_3^-)$ based upon the negative photolytic $^{15}\varepsilon$ (−45.3 ‰) is not observed nor does $\delta^{15}N(NO_3^-)$ show a sharp increase with the decreasing $w(NO_3^-)$ in the upper 10 cm. Furthermore, given the results from the inland pits, a higher degree of photolytic NO_3^- loss (i.e., the extent of photolysis) could be expected to be accompanied by more secondary oxidation in the condensed phase (e.g., Jacobi and Hilker, 2007), leading to a decrease of $\delta^{18}O(NO_3^-)$ in the upper snowpack. But there is a significant increasing trend of $\delta^{18}O(NO_3^-)$ in the upper 30 cm of snow (Fig. 7) and there is no relationship between $\delta^{15}N(NO_3^-)$ and $\delta^{18}O(NO_3^-)$ in the dataset as a whole or when divided by season. Thus, it is concluded that photolytic loss of NO_3^- at P1 is likely not influential.

If volatilization was driving the variability of $w(NO_3^-)$, a relationship between $w(NO_3^-)$ and $\delta^{15}N(NO_3^-)$ could be expected based on the theoretically calculated value for $^{15}\varepsilon$ (Table S2), but none is observed (Table 2). On the other hand, the $^{15}\varepsilon$ value at −20 °C reported from the Dome C experiment ($^{15}\varepsilon$ = −0.3 ‰) is effectively non-fractionating (Erbland et al., 2013). Based on this, it is difficult to attribute the isotopic variability in P1 to volatilization.

ACPD
14, 31943–31986, 2014

In summary, the observed variability in $w(NO_3^-)$ and isotopic composition cannot be explained by post-depositional processes in snow, given our current knowledge of isotopic fractionations of the processes discussed above. The observed large variations in the P1 isotopic and mass fraction data are more plausibly explained as presenting a NO_3^- source shift over different periods, which may be further corroborated by the changing relationship of $w(NO_3^-)$ vs. $\delta^{18}O(NO_3^-)$ between cold and warm seasons (Fig. 8b).

A number of studies have suggested that the stratosphere is the primary source of NO_3^- to the Antarctic ice sheet (Mulvaney and Wolff, 1993; Wagenbach et al., 1998; Savarino et al., 2007), with an estimated annual flux of $6.3 \pm 2.7 \times 10^7$ kg N a^{-1} (Muscari et al., 2003). As discussed by Savarino et al. (2007), interactions between NO_x and stratosphere ozone lead to some of the highest $\Delta^{17}O$ (and $\delta^{18}O$) of NO_3^- values, which have been thus far only observed in polar regions. It is notable that $\delta^{18}O(NO_3^-)$ values above 90 ‰ are all present in cold season snow, and $\delta^{18}O(NO_3^-)$ and $\Delta^{17}O(NO_3^-)$ (ranging from 69.5 to 105.3 ‰ and 25.2 to 42.9 ‰, respectively) in this period are comparable to the data of atmospheric NO_3^- (inorganic NO_3^- aerosol) in winter at the coastal East Antarctic Dumont d'Urville station (DDU; 66°40′ S, l40°01′ E), where the higher $\delta^{18}O(NO_3^-)$ and $\Delta^{17}O(NO_3^-)$ in winter is thought to be linked with stratospheric NO_3^- deposition (Savarino et al., 2007). The great enrichment of ^{18}O and ^{17}O in the cold season NO_3^- in P1 suggests that O atoms from stratospheric O_3 have been incorporated into NO_x and NO_3^- (R4-R6) that was subsequently deposited in snow as NO_3^-.

Interestingly, the highest $\delta^{18}O(NO_3^-)$ and $\Delta^{17}O(NO_3^-)$ values are all found in the most recent winter/spring in P1, namely 2012. This season was marked by much less stratospheric O_3 loss and a smaller O_3 hole extent than in previous seasons covered by the P1 snowpit; the mean 2012 O_3 hole area was 19 % smaller than the prior 3 year average, and the minimum O_3 concentration of 139.1DU detected by satellite was the highest on record since 1988 (based on data from the NASA Goddard Space Flight Center: http://ozonewatch.gsfc.nasa.gov/meteorology/annual_data.txt). This might support

ACPD
14, 31943–31986, 2014

that, where atmospheric NO_3^- is preserved in Antarctic snow, the O isotopes of NO_3^- could track stratospheric O_3 changes over time (McCabe et al., 2007).

The $\delta^{15}N(NO_3^-)$ in P1 cold season snow has a mean of 31.0 ± 14.5 ‰, which is much higher than that found in atmospheric NO_3^- at DDU (maximum of 10.8 ‰). Savarino et al. (2007) calculated that the isotopic signature of NO formed in the stratosphere would be 19 ± 3 ‰ based upon the estimated fractionation of N_2O upon decomposition. Based on the expectation that more than 90 % of stratospheric NO_y (sum of reactive nitrogen oxide compounds) is removed during denitrification, Savarino et al. (2007) further predicted that the $\delta^{15}N$ of NO is close to the $\delta^{15}N$ of NO_3^-. The much higher values found in coastal snow must then represent either a higher stratospheric $\delta^{15}N$ source value than predicted, or fractionation associated with chemistry, transport or deposition. The $\delta^{18}O$ of NO_3^- and the correlation of $\delta^{18}O(NO_3^-)$ and $\Delta^{17}O(NO_3^-)$ fit well within the range expected, and it is unlikely that significant fractionation associated with chemistry/transport/deposition would affect only $\delta^{15}N(NO_3^-)$ and not $\delta^{18}O(NO_3^-)$. Thus, a higher $\delta^{15}N(NO_3^-)$ value (or range) than 19 ‰ from stratospheric denitrification is needed to explain the P1 cold season data.

The warm season snow in P1 exhibits lower mean $\delta^{15}N$, $\delta^{18}O$ and $\Delta^{17}O$ of NO_3^- (15.1, 77.4 and 30.4 ‰, respectively). These lower values, and the occurrence of $\delta^{15}N(NO_3^-) < 0$ ‰ in warm seasons, are also consistent with the DDU atmospheric data (Savarino et al., 2007). The very low and negative $\delta^{15}N(NO_3^-)$ values found between October–December at DDU were interpreted as resulting from HNO_3 formed in the atmosphere from snow sourced NO_x emissions. Namely, the release of NO_x from photolysis of surface snow NO_3^- can explain these values because of the very large and negative $^{15}\varepsilon$ (see Sect. 4.1.1 above). The seasonally lowered O isotopic composition can then be explained as arising from the gas-phase oxidation of snow-sourced NO_x to HNO_3 predominantly by OH (R3), which would be expected to be the predominant pathway of HNO_3 formation during the warm season (Alexander et al., 2009).

ACPD
14, 31943–31986, 2014

While the mean values shown in Fig. 8a are representative of the seasonal shifts in the isotopic composition of NO_3^-, it is also clear from Fig. 7 that there is significant interannual variability. A recent adjoint modeling study suggested that $w(NO_3^-)$ in Antarctic snow was most sensitive to tropospheric sources of NO_x, primarily fossil fuel combustion, biogenic soil emissions and lightning, though snow emissions were not considered in the model (Lee et al., 2014). The isotopic signatures of NO_x sources and their relationship with the $\delta^{15}N$ of NO_3^- are poorly constrained, particularly in the Southern Hemisphere. For example, the $\delta^{15}N$ of NO_x from vehicle emissions in South Africa were consistently negative (Heaton, 1990) while that found in Switzerland was mostly positive.(Ammann et al., 1999). Fertilized soils in a laboratory study emitted NO_x with very low $\delta^{15}N$ (from −48.9 to −19.9 ‰) (Li and Wang, 2008), and lightning-sourced NO_x is expected to be near 0 ‰. Additionally, peroxyacetyl nitrate (PAN) is suggested as an important source of NO_x to the Antarctic atmosphere during the warm season (Lee et al., 2014). While no direct information is available in terms of the $\delta^{15}N$ of NO_x (or NO_3^-) produced from PAN decomposition, it has been suggested that this could explain sporadic high $\delta^{15}N$ of NO_3^- in the northern subtropical marine system (Altieri et al., 2013). Thus, it is not possible to link the observed changes in isotopic composition directly to NO_x emission sources. Still, qualitatively, and based on the combination of isotopes, the P1 snowpit data would agree with a varying relative contribution of tropospheric NO_x sources from year-to-year in the warm season. In the cold season, the data suggest that there is still an important degree of stratospheric influence on NO_3^- loading in Antarctic snow, particularly in 2012 when the O_3 hole was unusually small.

5 Conclusions

The purpose of this study was to investigate the effects of post-depositional processes on isotopic fractionation of NO_3^- at different depths in the snowpack, and to understand variation of NO_3^- isotopic composition in different environments on the

ACPD
14, 31943–31986, 2014

EAIS. In the EAIS interior, where accumulation rates are very low (group II snowpits; $< 55\,kg\,m^{-2}\,a^{-1}$), a higher degree of NO_3^- loss is found. The high values of $\delta^{15}N(NO_3^-)$ found in near-surface snow (i.e., top 25 cm) and the relationship between $w(NO_3^-)$ and $\delta^{15}N(NO_3^-)$ are consistent with a Rayleigh-type process and theoretically predicted $^{15}\varepsilon$ values for NO_3^- photolysis. The concurrent decreases in $\delta^{18}O(NO_3^-)$, however, are best explained as resulting from condensed-phase re-oxidation forming secondary NO_3^- that contains oxygen atoms derived from in situ H_2O (e.g., $\delta^{18}O(H_2O)$ of −50 ‰). This significantly decreases the $\delta^{18}O(NO_3^-)$ overall from what was originally deposited, and explains the positive relationship between $w(NO_3^-)$ and the $\delta^{18}O$ of NO_3^- (and therefore the positive observed $^{18}\varepsilon$ values). Interestingly, below 25 cm in the group II snowpits, a change in the relationship between $w(NO_3^-)$ and $\delta^{18}O(NO_3^-)$ is observed. These findings highlight the utility of the combined use of $\delta^{15}N(NO_3^-)$ and $\delta^{18}O(NO_3^-)$ for detecting post-depositional processing of NO_3^- and the difficulty in predicting the isotopic composition of NO_3^- at depth based on the fractionation of near-surface NO_3^- alone. We find that in both group II and group I snowpits (accumulation $> 91\,kg\,m^{-2}\,a^{-1}$), $w(NO_3^-)$, $\delta^{15}N(NO_3^-)$, and $\delta^{18}O(NO_3^-)$ cannot be fit by a simple exponential decrease model. In the case of the group II snowpits, a significant negative relationship is observed between $w(NO_3^-)$ and $\delta^{18}O(NO_3^-)$ at depths between 100–200 cm. In the case of the group I snowpits, seasonal variability is found in $w(NO_3^-)$, $\delta^{15}N$, $\delta^{18}O$, and $\Delta^{17}O$ of NO_3^- throughout the profiles. We suggest that the seasonality observed in higher accumulation, more coastal EAIS sites is driven by the influence of NO_3^- sources. The best explanation for the range of values seen, given current knowledge, is the importance of stratospheric production of atmospheric NO_3^- in the cold season compared to more tropospheric NO_x source influence in the warm season.

ACPD
14, 31943–31986, 2014

The Supplement related to this article is available online at doi:10.5194/acpd-14-31943-2014-supplement.

Acknowledgements. This research was supported by the National Science Foundation of China (Grant Nos. 41206188, 41476169), the US National Science Foundation Antarctic Glaciology Program (Grant No. 1246223) and Young Scientists Foundation of the State Oceanic Administration of China (Grant No. 2012532). We are also grateful to Ruby Ho at Brown University and the 29th CHINARE inland members for technical support and assistance, and two anonymous reviewers for their helpful comments.

References

Alexander, B., Savarino, J., Kreutz, K. J., and Thiemens, M.: Impact of preindustrial biomass-burning emissions on the oxidation pathways of tropospheric sulfur and nitrogen, J. Geophys. Res., 109, D08303, doi:10.1029/2003JD004218, 2004.

Alexander, B., Hastings, M. G., Allman, D. J., Dachs, J., Thornton, J. A., and Kunasek, S. A.: Quantifying atmospheric nitrate formation pathways based on a global model of the oxygen isotopic composition ($\Delta^{17}O$) of atmospheric nitrate, Atmos. Chem. Phys., 9, 5043–5056, doi:10.5194/acp-9-5043-2009, 2009.

Altieri, K., Hastings, M., Gobel, A., Peters, A., and Sigman, D.: Isotopic composition of rainwater nitrate at Bermuda: The influence of air mass source and chemistry in the marine boundary layer, J. Geophys. Res., 118, 11304–11316, 2013.

Ammann, M., Siegwolf, R., Pichlmayer, F., Suter, M., Saurer, M., and Brunold, C.: Estimating the uptake of traffic-derived NO_2 from ^{15}N abundance in Norway spruce needles, Oecologia, 118, 124–131, 1999.

Böhlke, J., Mroczkowski, S., and Coplen, T.: Oxygen isotopes in nitrate: new reference materials for ^{18}O: ^{17}O: ^{16}O measurements and observations on nitrate-water equilibration, Rapid Commun. Mass. Sp., 17, 1835–1846, 2003.

Berhanu, T. A., Meusinger, C., Erbland, J., Jost, R., Bhattacharya, S., Johnson, M. S., and Savarino, J.: Laboratory study of nitrate photolysis in Antarctic snow. II. Isotopic effects and wavelength dependence, J. Chem. Phys., 140, 244306, doi:10.1063/1.4882899, 2014.

ACPD
14, 31943–31986, 2014

Blunier, T., Floch, G., Jacobi, H.-W., and Quansah, E.: Isotopic view on nitrate loss in Antarctic surface snow, Geophys. Res. Lett., 32, L13501, doi:10.1029/2005GL023011, 2005.
Boxe, C., Colussi, A., Hoffmann, M., Murphy, J., Wooldridge, P., Bertram, T., and Cohen, R.: Photochemical production and release of gaseous NO_2 from nitrate-doped water ice, J. Phys. Chem., 109, 8520–8525, 2005.
Buffen, A. M., Hastings, M. G., Thompson, L. G., and Mosley-Thompson, E.: Investigating the preservation of nitrate isotopic composition in a tropical ice core from the Quelccaya Ice Cap, Peru, J. Geophys. Res., 119, 2674–2697, doi:10.1002/2013JD020715, 2014.
Bunton, C., Halevi, E., and Llewellyn, D.: Oxygen exchange between nitric acid and water. Part I, J. Chem. Soc., 4913–4916, doi:10.1039/jr9520004913, 1952.
Casciotti, K., Sigman, D., Hastings, M. G., Böhlke, J., and Hilkert, A.: Measurement of the oxygen isotopic composition of nitrate in seawater and freshwater using the denitrifier method, Anal. Chem., 74, 4905–4912, 2002.
Chu, L. and Anastasio, C.: Quantum yields of hydroxyl radical and nitrogen dioxide from the photolysis of nitrate on ice, J. Phys. Chem., 107, 9594–9602, 2003.
Criss, R. E.: Principles of Stable Isotope Distribution, Oxford University Press, New York, 254 pp., 1999.
Delmas, R., Serca, D., and Jambert, C.: Global inventory of NO_x sources, Nutr. Cycl. Agroecosys., 48, 51–60, 1997.
Dibb, J. E. and Fahnestock, M.: Snow accumulation, surface height change, and firn densification at Summit, Greenland: insights from 2 years of in situ observation, J. Geophys. Res., 109, D24113, doi:10.1029/2003JD004300, 2004.
Dibb, J. E., Arsenault, M., Peterson, M. C., and Honrath, R. E.: Fast nitrogen oxide photochemistry in Summit, Greenland snow, Atmos. Environ., 36, 2501–2511, 2002.
Ding, M., Xiao, C., Jin, B., Ren, J., Qin, D., and Sun, W.: Distribution of $\delta^{18}O$ in surface snow along a transect from Zhongshan Station to Dome A, East Antarctica, Chinese Sci. Bull., 55, 2709–2714, 2010.
Ding, M., Xiao, C., Li, Y., Ren, J., Hou, S., Jin, B., and Sun, B.: Spatial variability of surface mass balance along a traverse route from Zhongshan station to Dome A, Antarctica, J. Glaciol., 57, 658–666, 2011.
Dubowski, Y., Colussi, A., and Hoffmann, M.: Nitrogen dioxide release in the 302 nm band photolysis of spray-frozen aqueous nitrate solutions. Atmospheric implications, J. Phys. Chem., 105, 4928–4932, 2001.

ACPD
14, 31943–31986, 2014

Elliott, E. M., Kendall, C., Wankel, S. D., Burns, D. A., Boyer, E. W., Harlin, K., Bain, D. J., and Butler, T. J.: Nitrogen isotopes as indicators of NO_x source contributions to atmospheric nitrate deposition across the midwestern and northeastern United States, Environ. Sci. Technol., 41, 7661–7667, doi:10.1021/es070898t, 2007.

Erbland, J., Vicars, W. C., Savarino, J., Morin, S., Frey, M. M., Frosini, D., Vince, E., and Martins, J. M. F.: Air–snow transfer of nitrate on the East Antarctic Plateau – Part 1: Isotopic evidence for a photolytically driven dynamic equilibrium in summer, Atmos. Chem. Phys., 13, 6403–6419, doi:10.5194/acp-13-6403-2013, 2013.

Fibiger, D. L., Hastings, M. G., Dibb, J. E., and Huey, L. G.: The preservation of atmospheric nitrate in snow at Summit, Greenland, Geophys. Res. Lett., 40, 3484–3489, 2013.

Frey, M. M., Savarino, J., Morin, S., Erbland, J., and Martins, J. M. F.: Photolysis imprint in the nitrate stable isotope signal in snow and atmosphere of East Antarctica and implications for reactive nitrogen cycling, Atmos. Chem. Phys., 9, 8681–8696, doi:10.5194/acp-9-8681-2009, 2009.

Frey, M. M., Brough, N., France, J. L., Anderson, P. S., Traulle, O., King, M. D., Jones, A. E., Wolff, E. W., and Savarino, J.: The diurnal variability of atmospheric nitrogen oxides (NO and NO_2) above the Antarctic Plateau driven by atmospheric stability and snow emissions, Atmos. Chem. Phys., 13, 3045–3062, doi:10.5194/acp-13-3045-2013, 2013.

Grannas, A. M., Jones, A. E., Dibb, J., Ammann, M., Anastasio, C., Beine, H. J., Bergin, M., Bottenheim, J., Boxe, C. S., Carver, G., Chen, G., Crawford, J. H., Dominé, F., Frey, M. M., Guzmán, M. I., Heard, D. E., Helmig, D., Hoffmann, M. R., Honrath, R. E., Huey, L. G., Hutterli, M., Jacobi, H. W., Klán, P., Lefer, B., McConnell, J., Plane, J., Sander, R., Savarino, J., Shepson, P. B., Simpson, W. R., Sodeau, J. R., von Glasow, R., Weller, R., Wolff, E. W., and Zhu, T.: An overview of snow photochemistry: evidence, mechanisms and impacts, Atmos. Chem. Phys., 7, 4329–4373, doi:10.5194/acp-7-4329-2007, 2007.

Hastings, M. G.: Evaluating source, chemistry and climate change based upon the isotopic composition of nitrate in ice cores, IOP C. Ser. Earth Env., 9, 012002, doi:10.1088/1755-1315/9/1/012002, 2010.

Hastings, M. G., Sigman, D. M., and Lipschultz, F.: Isotopic evidence for source changes of nitrate in rain at Bermuda, J. Geophys. Res., 108, 4790, doi:10.1029/2003JD003789, 2003.

Hastings, M. G., Steig, E., and Sigman, D.: Seasonal variations in N and O isotopes of nitrate in snow at Summit, Greenland: implications for the study of nitrate in snow and ice cores, J. Geophys. Res., 109, D20306, doi:10.1029/2004JD004991, 2004.

ACPD
14, 31943–31986, 2014

Hastings, M. G., Jarvis, J. C., and Steig, E. J.: Anthropogenic impacts on nitrogen isotopes of ice-core nitrate, Science, 324, 1288–1288, 2009.
Heaton, T. H. E.: $^{15}N/^{14}N$ ratios of NO_x from vehicle engines and coal-fired power stations, Tellus B, 42, 304–307, 1990.
Hutterli, M. A., McConnell, J. R., Chen, G., Bales, R. C., Davis, D. D., and Lenschow, D. H.: Formaldehyde and hydrogen peroxide in air, snow and interstitial air at South Pole, Atmos. Environ., 38, 5439–5450, 2004.
Jacobi, H.-W. and Hilker, B.: A mechanism for the photochemical transformation of nitrate in snow, J. Photochem. Photobiol. A, 185, 371–382, 2007.
Johnsen, S. J., Clausen, H. B., Dansgaard, W., Gundestrup, N. S., Hammer, C. U., Andersen, U., Andersen, K. K., Hvidberg, C. S., Dahl-Jensen, D., and Steffensen, J. P.: The $\delta^{18}O$ record along the Greenland Ice Core Project deep ice core and the problem of possible Eemian climatic instability, J. Geophys. Res., 102, 26397–26410, 1997.
Kaiser, J., Hastings, M. G., Houlton, B. Z., Röckmann, T., and Sigman, D. M.: Triple oxygen isotope analysis of nitrate using the denitrifier method and thermal decomposition of N_2O, Anal. Chem., 79, 599–607, 2007.
Laepple, T., Werner, M., and Lohmann, G.: Synchronicity of Antarctic temperatures and local solar insolation on orbital timescales, Nature, 471, 91–94, 2011.
Lee, D., Köhler, I., Grobler, E., Rohrer, F., Sausen, R., Gallardo-Klenner, L., Olivier, J., Dentener, F., and Bouwman, A.: Estimations of global NO_x, emissions and their uncertainties, Atmos. Environ., 31, 1735–1749, 1997.
Lee, H.-M., Henze, D. K., Alexander, B., and Murray, L. T.: Investigating the sensitivity of surface-level nitrate seasonality in Antarctica to primary sources using a global model, Atmos. Environ., 89, 757–767, 2014.
Legrand, M., Preunkert, S., Frey, M., Bartels-Rausch, Th., Kukui, A., King, M. D., Savarino, J., Kerbrat, M., and Jourdain, B.: Large mixing ratios of atmospheric nitrous acid (HONO) at Concordia (East Antarctic Plateau) in summer: a strong source from surface snow?, Atmos. Chem. Phys., 14, 9963–9976, doi:10.5194/acp-14-9963-2014, 2014.
Li, D. and Wang, X.: Nitrogen isotopic signature of soil-released nitric oxide (NO) after fertilizer application, Atmos. Environ., 42, 4747–4754, 2008.
Madronich, S. and Flocke, S.: The role of solar radiation in atmospheric chemistry, in: Handbook of Environmental Chemistry, edited by: Boule, P., Springer Verlag, Heidelberg, 1–26, 1998.

ACPD
14, 31943–31986, 2014

Mayewski, P. A. and Legrand, M. R.: Recent increase in nitrate concentration of Antarctic snow, Nature, 346, 258–260, 1990.
McCabe, J., Boxe, C., Colussi, A., Hoffmann, M., and Thiemens, M.: Oxygen isotopic fractionation in the photochemistry of nitrate in water and ice, J. Geophys. Res., 110, D15310, doi:10.1029/2004JD005484, 2005.
McCabe, J. R., Thiemens, M. H., and Savarino, J.: A record of ozone variability in South Pole Antarctic snow: role of nitrate oxygen isotopes, J. Geophys. Res., 112, D12303, doi:10.1029/2006JD007822, 2007.
Michalski, G., Savarino, J., Böhlke, J., and Thiemens, M.: Determination of the total oxygen isotopic composition of nitrate and the calibration of a $\Delta^{17}O$ nitrate reference material, Anal. Chem., 74, 4989–4993, 2002.
Michalski, G., Scott, Z., Kabiling, M., and Thiemens, M. H.: First measurements and modeling of $\Delta^{17}O$ in atmospheric nitrate, Geophys. Res. Lett., 30, 1870, doi:10.1029/2003GL017015, 2003.
Morin, S., Savarino, J., Frey, M. M., Yan, N., Bekki, S., Bottenheim, J. W., and Martins, J. M.: Tracing the origin and fate of NO_x in the Arctic atmosphere using stable isotopes in nitrate, Science, 322, 730–732, 2008.
Mulvaney, R. and Wolff, E.: Evidence for winter/spring denitrification of the stratosphere in the nitrate record of Antarctic firn cores, J. Geophys. Res., 98, 5213–5220, 1993.
Mulvaney, R., Wagenbach, D., and Wolff, E. W.: Postdepositional change in snowpack nitrate from observation of year-round near-surface snow in coastal Antarctica, J. Geophys. Res., 103, 11021–11031, 1998.
Muscari, G., de Zafra, R. L., and Smyshlyaev, S.: Evolution of the NO_y–N_2O correlation in the Antarctic stratosphere during 1993 and 1995, J. Geophys. Res., 108, 4428, doi:10.1029/2002JD002871, 2003.
Röthlisberger, R., Hutterli, M. A., Sommer, S., Wolff, E. W., and Mulvaney, R.: Factors controlling nitrate in ice cores: evidence from the Dome C deep ice core, J. Geophys. Res., 105, 20565–20572, 2000.
Röthlisberger, R., Hutterli, M. A., Wolff, E. W., Mulvaney, R., Fischer, H., Bigler, M., Goto-Azuma, K., Hansson, M. E., Ruth, U., and Siggaard-Andersen, M.-L.: Nitrate in Greenland and Antarctic ice cores: a detailed description of post-depositional processes, Ann. Glaciol., 35, 209–216, 2002.

ACPD
14, 31943–31986, 2014

Sato, K., Takenaka, N., Bandow, H., and Maeda, Y.: Evaporation loss of dissolved volatile substances from ice surfaces, J. Phys. Chem., 112, 7600–7607, 2008.
Savarino, J., Kaiser, J., Morin, S., Sigman, D. M., and Thiemens, M. H.: Nitrogen and oxygen isotopic constraints on the origin of atmospheric nitrate in coastal Antarctica, Atmos. Chem. Phys., 7, 1925–1945, doi:10.5194/acp-7-1925-2007, 2007.
Sigman, D. M., Casciotti, K. L., Andreani, M., Barford, C., Galanter, M., and Böhlke, J. K.: A bacterial method for the nitrogen isotopic analysis of nitrate in seawater and freshwater, Anal. Chem., 73, 4145–4153, 2001.
Traversi, R., Becagli, S., Castellano, E., Cerri, O., Morganti, A., Severi, M., and Udisti, R.: Study of Dome C site (East Antartica) variability by comparing chemical stratigraphies, Microchem. J., 92, 7–14, 2009.
Vagenhach, D., Graf, V., Minikin, A., Trefzer, U., Kipfstuhl, J., Oerter, H., and Blindow, N.: Reconnaissance of chemical and isotopic firn properties on top of Berkner Island, Antarctica, Ann. Glaciol., 20, 307–312, 1994.
Vicars, W. C. and Savarino, J.: Quantitative constraints on the ^{17}O-excess (Δ^{17}O) signature of surface ozone: ambient measurements from 50° N to 50° S using the nitrite-coated filter technique, Geochim. Cosmochim. Ac., 135, 270–287, 2014.
Wagenbach, D., Legrand, M., Fischer, H., Pichlmayer, F., and Wolff, E. W.: Atmospheric near-surface nitrate at coastal Antarctic sites, J. Geophys. Res., 103, 11007–11020, 1998.
Warneck, P. and Wurzinger, C.: Product quantum yields for the 305 nm photodecomposition of nitrate in aqueous solution, J. Phys. Chem., 92, 6278–6283, 1988.
Warren, S. G., Brandt, R. E., and Grenfell, T. C.: Visible and near-ultraviolet absorption spectrum of ice from transmission of solar radiation into snow, Appl. Optics, 45, 5320–5334, 2006.
Wolff, E. W.: Nitrate in polar ice, in: Ice Core Studies of Global Biogeochemical Cycles, edited by: Delmas, R. J., Springer, New York, 195–224, 1995.
Wolff, E. W., Jones, A. E., Bauguitte, S. J.-B., and Salmon, R. A.: The interpretation of spikes and trends in concentration of nitrate in polar ice cores, based on evidence from snow and atmospheric measurements, Atmos. Chem. Phys., 8, 5627–5634, doi:10.5194/acp-8-5627-2008, 2008.
Wolff, E. W., Bigler, M., Curran, M., Dibb, J., Frey, M., Legrand, M., and McConnell, J.: The Carrington event not observed in most ice core nitrate records, Geophys. Res. Lett., 39, L08503, doi:10.1029/2012GL051603, 2012.

ACPD
14, 31943–31986, 2014

Zatko, M. C., Grenfell, T. C., Alexander, B., Doherty, S. J., Thomas, J. L., and Yang, X.: The influence of snow grain size and impurities on the vertical profiles of actinic flux and associated NO_x emissions on the Antarctic and Greenland ice sheets, Atmos. Chem. Phys., 13, 3547–3567, doi:10.5194/acp-13-3547-2013, 2013.

ACPD
14, 31943–31986, 2014

Table 1. Statistics of snow $w(NO_3^-)$, $\delta^{15}N$ and $\delta^{18}O$ of NO_3^- in the seven snowpits collected from East Antarctica.

Parameter	Snowpit	P1	P2	P3	P4	P5	P6	P7
$w(NO_3^-)$, ng g^{-1}	Mean	46.6	79.1	91.6	56.5	42.6	83.7	23.8
	Min	26.7	38.5	59.5	24.1	14.6	35.4	7.9
	Max	97.1	173.0	266.3	151.3	175.1	202.6	373.8
	SD	17.6	25.4	35.3	21.4	31.1	39.9	46.4
$\delta^{15}N$, ‰	Mean	24.7	23.0	21.3	133.6	196.3	160.9	335.2
	Min	−14.8	−12.1	−2.2	15.5	48.0	50.8	111.0
	Max	59.4	70.8	39.9	184.2	280.4	236.8	460.8
	SD	17.5	17.9	9.0	31.7	48.2	47.7	52.5
$\delta^{18}O$, ‰	Mean	82.5	81.1	85.1	59.9	54.4	52.5	48.9
	Min	66.7	69.9	52.5	45.8	42.7	36.2	16.8
	Max	105.3	96.8	111.2	75.6	82.2	81.9	84.0
	SD	11.0	7.7	16.2	7.0	9.0	10.1	12.1

ACPD
14, 31943–31986, 2014

Table 2. Observed fractionation constants for ^{15}N and ^{18}O of NO_3^- calculated for different snow layer depths from the linear regression of $\ln(\delta_{snow}+1)$ vs. $\ln(w_{snow})$ in Eq. (2). Four different depth intervals were selected for calculating ε: 0–25, 25–100, 100 cm to the pit base and the entire pit. Also given are the r^2 values and the significance level, p, where bolded values represents $p < 0.05$.

Snow pit	Depth	^{15}N			^{18}O		
		$^{15}\varepsilon$, ‰	p	r^2	$^{18}\varepsilon$, ‰	p	r^2
P1	0–25 cm	2.5	0.29	0.16	−13.7	0.11	0.33
	25–100 cm	**−61.7**	**0.00**	**0.44**	**32.3**	**0.00**	**0.39**
	100–bottom	18.7	0.14	0.15	−8.2	0.08	0.21
	Entire	−14.0	0.05	0.08	−1.8	0.38	0.00
P2	0–25 cm	−16.3	0.50	0.12	−0.4	0.87	0.01
	25–100 cm	25.0	0.09	0.20	7.3	0.19	0.12
	100–bottom	21.5	0.20	0.09	**11.2**	**0.02**	**0.29**
	Entire	11.9	0.20	0.04	6.9	0.06	0.09
P3	**0–25 cm**	**−35.7**	**0.01**	**0.88**	−22.0	0.17	0.41
	25–100 cm	8.3	0.37	0.06	−7.2	0.58	0.02
	100–bottom	12.3	0.32	0.06	13.5	0.48	0.03
	Entire	−1.2	0.81	0.00	15.4	0.06	0.09
P4	**0–25 cm**	**−78.1**	**0.00**	**0.91**	**15.9**	**0.00**	**0.78**
	25–100 cm	**−50.1**	**0.00**	**0.34**	**6.2**	**0.05**	**0.11**
	100–bottom	**−56.0**	**0.00**	**0.70**	**−3.4**	**0.01**	**0.13**
	Entire	**−58.7**	**0.00**	**0.58**	1.7	0.43	0.01
P5	**0–25 cm**	**−84.4**	**0.00**	**0.63**	**28.8**	**0.01**	**0.44**
	25–100 cm	**−52.5**	**0.00**	**0.60**	**−2.5**	**0.03**	**0.12**
	100–bottom	27.3	0.05	0.08	**−9.6**	**0.02**	**0.11**
	Entire	**−56.9**	**0.00**	**0.58**	0.4	0.99	0.00
P6	**0–25 cm**	**−54.0**	**0.00**	**0.82**	**18.0**	**0.00**	**0.64**
	25–100 cm	**−46.4**	**0.03**	**0.16**	7.9	0.15	0.07
	100–bottom	**−61.3**	**0.00**	**0.61**	**−7.8**	**0.00**	**0.22**
	Entire	**−76.8**	**0.00**	**0.69**	**11.3**	**0.00**	**0.27**
P7	**0–25 cm**	**−59.2**	**0.00**	**0.86**	**17.8**	**0.00**	**0.74**
	25–100 cm	**34.4**	**0.01**	**0.24**	**−9.4**	**0.00**	**0.36**
	100–bottom	20.7	0.15	0.03	10.0	0.05	0.06
	Entire	**−31.5**	**0.00**	**0.25**	−0.7	0.69	0.00

ACPD
14, 31943–31986, 2014

Table 3. Asymptotic values of $w(NO_3^-)$, $\delta^{15}N$ and $\delta^{18}O$ of NO_3^- calculated based on five different snow depth intervals (0–25 cm, 0–60 cm, 0–80 cm, 0–100 cm and entire depth) of each snowpit. p is the significance level of observed data fitted using the exponential decrease regression Eq. (6), and r^2 denotes squared correlation coefficient of observed data compared to the regression model predicted values.

Snowpit	Depth	$w(NO_3^-)_{(as.)}$, ng g^{-1}			$\delta^{15}N_{(as.)}$, ‰			$\delta^{18}O_{(as.)}$, ‰		
		$w(NO_3^-)$	p	r^2	$\delta^{15}N$	p	r^2	$\delta^{18}O$	p	r^2
P4	Entire	53.6	0.00	0.41	137.2	0.00	0.27	46.8	0.00	0.45
	−100 cm	54.5	0.00	0.58	144.3	0.00	0.51	54.5	0.00	0.29
	−80 cm	55.3	0.00	0.57	146.3	0.00	0.55	53.6	0.00	0.34
	−60 cm	45.3	0.00	0.83	158.4	0.00	0.82	51.6	0.00	0.58
	−25 cm	27.2	0.00	0.93	180.5	0.00	0.95	44.5	0.00	0.89
P5	Entire	25.7	0.00	0.93	220.3	0.00	0.75	53.3	0.00	0.24
	−100 cm	25.8	0.00	0.93	254.6	0.00	0.92	48.2	0.00	0.65
	−80 cm	19.7	0.00	0.92	282.0	0.00	0.91	46.9	0.00	0.69
	−60 cm	39.9	0.00	0.92	277.9	0.00	0.89	46.0	0.00	0.71
	−25 cm	40.8	0.00	0.88	176.5	0.00	0.72	35.4	0.00	0.65
P6	Entire	34.1	0.00	0.80	256.4	0.00	0.72	47.6	0.00	0.59
	−100 cm	40.4	0.00	0.65	179.7	0.00	0.43	39.9	0.00	0.61
	−80 cm	55.0	0.00	0.52	196.0	0.00	0.37	20.9	0.00	0.59
	−60 cm	121.4	0.00	0.39	160.1	0.00	0.42	22.7	0.00	0.54
	−25 cm	123.4	0.01	0.53	96.5	0.31	0.11	69.9	0.27	0.14
P7	Entire	14.1	0.00	0.97	344.5	0.00	0.47	48.3	0.00	0.10
	−100 cm	17.9	0.00	0.97	383.8	0.00	0.75	33.9	0.00	0.64
	−80 cm	20.9	0.00	0.97	406.2	0.00	0.83	31.5	0.00	0.73
	−60 cm	23.3	0.00	0.97	448.7	0.00	0.86	29.7	0.00	0.75
	−25 cm	26.1	0.00	0.97	287.7	0.00	0.86	34.2	0.00	0.73

ACPD
14, 31943–31986, 2014

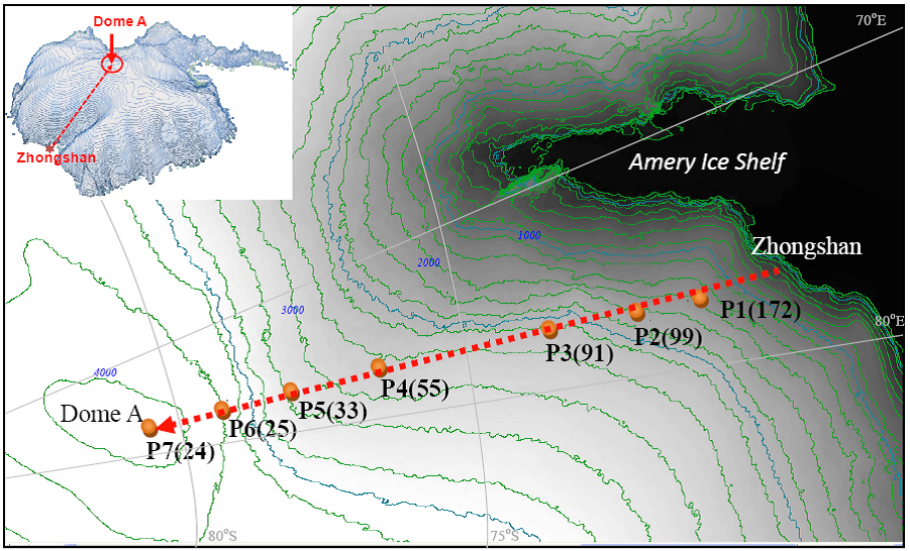

Figure 1. Snowpit locations sampled during the 2012/13 Chinese National Antarctic Research Expedition (CHINARE) inland traverse. The numbers in parentheses denote the annual snow accumulation rates ($kg\,m^{-2}\,a^{-1}$) which are extended to 2013 from bamboo stick field measurements (Ding et al., 2011).

ACPD
14, 31943–31986, 2014

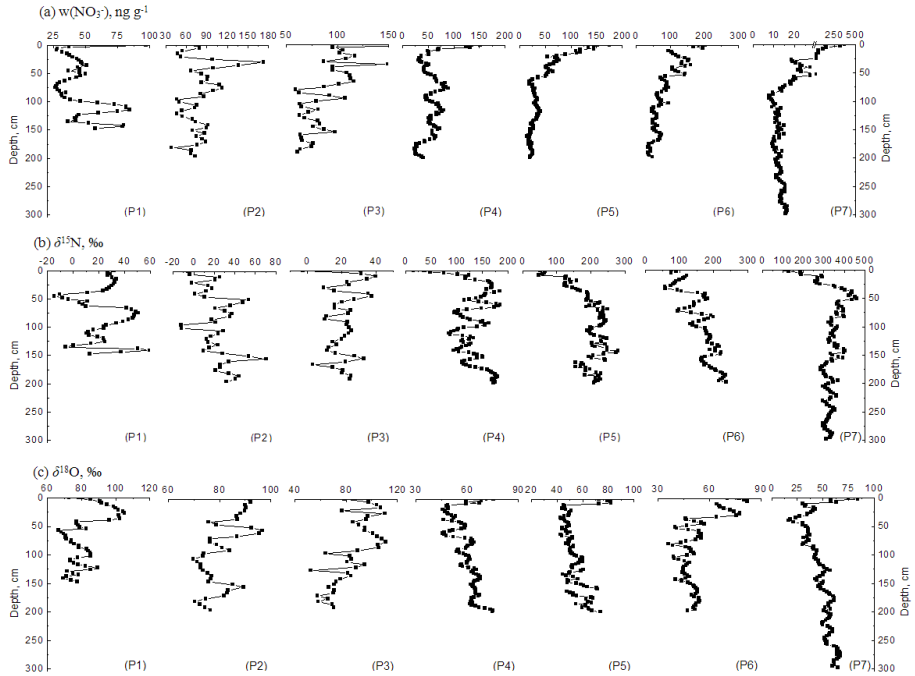

Figure 2. Detailed profiles of $w(NO_3^-)$ **(a)** and isotopic composition $\delta^{15}N$ **(b)** and $\delta^{18}O$ of NO_3^- (c) in the P1–P7 snowpits.

ACPD
14, 31943–31986, 2014

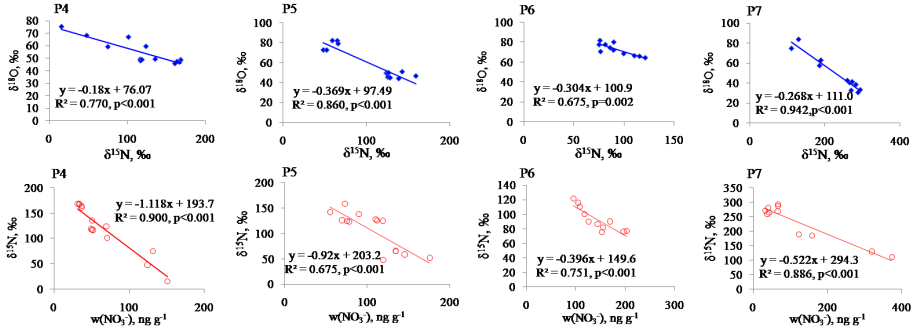

Figure 3. Linear relationships for P4–P7 between $\delta^{18}O$ (top row) and $\delta^{15}N$ (bottom row) of NO_3^- with $w(NO_3^-)$ in the topmost 25 cm of the snowpits. Least squares regressions are shown and are all significant at $p < 0.01$.

ACPD
14, 31943–31986, 2014

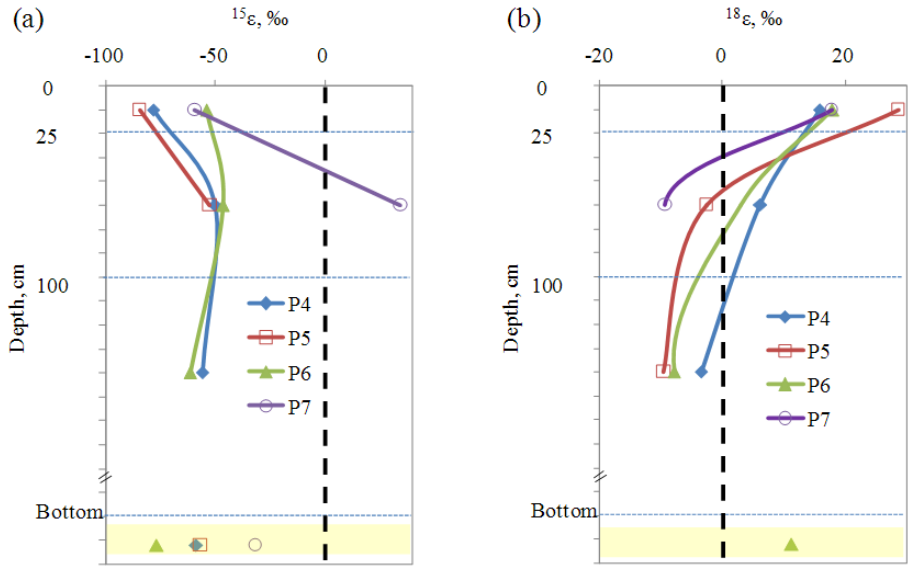

Figure 4. Observed fractionation constants, $^{15}\varepsilon$ and $^{18}\varepsilon$, calculated from the group II snowpits using three different snow depth intervals (0–25 cm, 25–100 and 100 cm–bottom. The ε values displayed in the shaded area are those calculated from the entire snowpit (0–bottom). Only statistically significant ε values ($p < 0.05$) are shown.

ACPD
14, 31943–31986, 2014

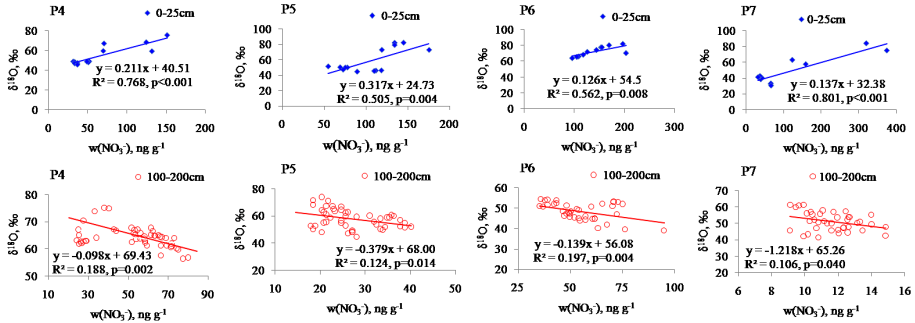

Figure 5. Relationship between $\delta^{18}O$ of NO_3^- and $w(NO_3^-)$ in the upper 25 cm (top row) and 100–200 cm (bottom row) in the group II snowpits. Least squares regressions are shown and are all significant at $p < 0.05$.

ACPD
14, 31943–31986, 2014

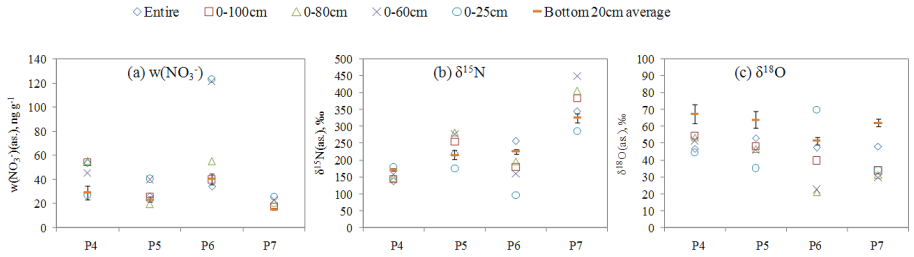

Figure 6. Predicted, asymptotic values of $w(NO_3^-)$, $\delta^{15}N$ and $\delta^{18}O$ of NO_3^- for the group II snowpits using five different snow depth intervals via Eq. (6): 0–25 cm (blue circle), 0–60 cm (purple x), 0–80 cm (green triangle), 0–100 cm (red square) and the entire snowpit (blue diamond). Means and SDs (1σ) of the observed data in the bottom 20 cm of each pit are also shown (orange bar).

ACPD
14, 31943–31986, 2014

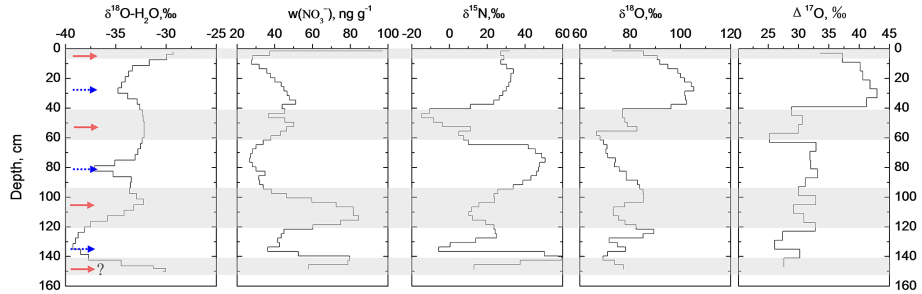

Figure 7. Seasonality in $w(NO_3^-)$, $\delta^{15}N$, $\delta^{18}O$ and $\Delta^{17}O$ of NO_3^- in the P1 snowpit. Red solid arrows and blue dashed arrows represent the middle of the identified warm and cold seasons, respectively, and shaded areas denote warm seasons (see text). One seasonal cycle represents one $\delta^{18}O(H_2O)$ peak to the next. Seasonal assignment of snow near the pit base is subject to uncertainty due to the limited coverage and absent comparison with a preceding cold season.

ACPD
14, 31943–31986, 2014

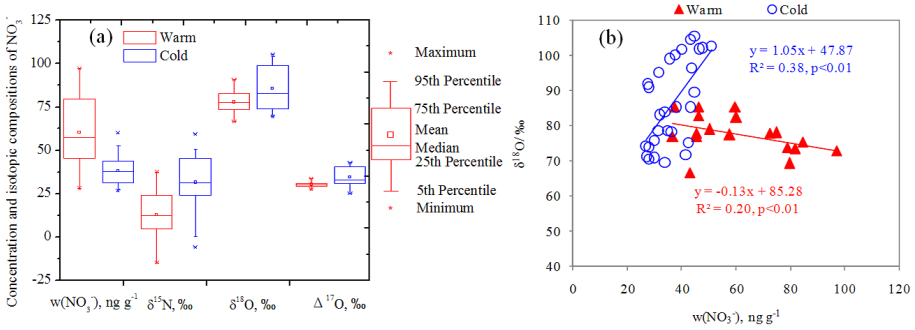

Figure 8. $w(NO_3^-)$, $\delta^{15}N$, $\delta^{18}O$ and $\Delta^{17}O$ of NO_3^- in warm and cold season samples from snowpit P1. Summary statistics by season are shown in **(a)**, and the seasonal relationships between $w(NO_3^-)$ and $\delta^{18}O$ of NO_3^- are shown in **(b)**.

ACPD
14, 31943–31986, 2014